

Structure Dependent Product Selectivity for CO₂ Electroreduction on ZnO Derived Catalysts

Kai Han,^[a] Peter Ngene,^[a] and Petra de Jongh^{*[a]}

Electrochemical conversion of CO₂ is an attractive alternative to releasing it to the atmosphere. Catalysts derived from electroreduction of metal oxides are often more active than when starting with metallic phase catalyst. The origin of this effect is not yet clear. Using ZnO nanorods, we show that the initial structure of the oxide as well as the electrolyte medium have a profound impact on the structure of the catalytic active Zn phase, and thereby the selectivity of the catalysts. ZnO nanorods with various aspect ratios were electrochemically reduced

in different electrolytes leading to metallic Zn with different structures; a sponge-like structure, nanorods and nanoplates. The sponge-like Zn produced syngas with H₂:CO = 2, and some formate, the nanorods produced only syngas with H₂:CO = 1, while Zn nanoplates exhibited 85% selectivity towards CO. These results open a pathway to design new electrocatalysts with optimized properties by modifying the structure of the starting material and the electroreduction medium.

Introduction

Electroreduction of CO₂ and protons to fuels and chemicals is a potential pathway to alleviate our dependence on fossil fuels.^[1–3] However, CO₂ reduction has a high activation barrier, and thus requires a large overpotential.^[4] Furthermore, the proton reduction reaction strongly competes and often limits the Faradaic efficiency to carbon-containing products.^[5] Therefore, an efficient catalyst is essential. Commonly, CO is believed to be an important intermediate for hydrocarbon production.^[6,7] In fact, materials that weakly bind CO mainly release CO, while the ones with medium CO binding strength can generate a mixture of hydrocarbon products, and the ones with strong CO binding hardly catalyze CO₂ reduction. Among the reported catalysts, Au,^[8,9] Ag,^[10,11] Pd^[12,13] and Cu^[14,15] are most frequently studied. Au and Ag preferentially produce CO with relatively low overpotential. Cu is the only catalyst able to produce C1–C3 hydrocarbon products with appreciable Faradaic efficiency, while Pd based catalysts can be used to produce syngas. As an alternative to noble metals, the earth-abundant Zn possesses a quite low CO binding energy (0.12 eV), and several studies have demonstrated that Zn is an interesting candidate for electrochemical reduction of CO₂ to CO or formate.^[16–20]

In 1985, Hori *et al* reported the efficiency of CO₂ reduction on various metal catalysts, and demonstrated that Zn produced CO with 63.3% Faradaic efficiency at current density of 5.5 mA/


cm² in CO₂ saturated 0.5 M KHCO₃.^[17] Since then, various treatments were reported to tune the structure of Zn-based electrocatalysts and their performance.^[16,19] Recently, a metallic Zn catalyst with a hierarchical hexagonal shape was shown to achieve a high CO₂ to CO conversion efficiency (FE = 95% at –1.05 V in 0.5 M KCl), as well as a high stability (5% activity loss in 30 h).^[19] According to DFT calculations, the Zn (101) facet can more effectively stabilize the *COOH intermediate than the Zn (002) facet during CO₂ reduction, leading to a lower reduction potential for CO₂ to CO. Zn-based catalysts with other structures have been prepared and their catalytic properties tested.^[20,21] Electrochemically deposited Zn on a Cu foam catalysts with various ratios of Zn (101) and Zn (002) facets led to different H₂:CO ratios under the same conditions.^[20]

In addition to metallic Zn catalysts, also ZnO catalysts with different morphologies were reported in literature.^[16,22] For instance, hydrothermally prepared ZnO nanosheets were shown to exhibit a high CO Faradaic efficiency (90% at –1.0 V vs RHE in 0.1 M KHCO₃).^[16] The reduction of metal oxide into a metallic phase under operational conditions is common.^[23–26] For ZnO around –0.7 V vs RHE is the potential below which thermodynamically metallic Zn is the most stable state.^[27] In other words, most of the catalysts designated as ZnO catalysts are in fact fully or partially reduced to metallic Zn under CO₂ reduction conditions.

Although it is known that the structure of the reduced phase can have a strong influence on the selectivity of the catalysts,^[19] the influence of the initial structure of the metal oxide phase and the reducing environment on the structure, and hence performance of the metallic phase, has not been yet reported in detail. We prepared ZnO nanorod catalysts of different aspect ratios. During CO₂ reduction, the ZnO nanorods were converted to different morphologies depending on the experimental conditions and the initial size of the nanorods, leading also to distinctly different catalytic performance.

[a] Dr. K. Han, Dr. P. Ngene, Prof. Dr. P. de Jongh
Inorganic Chemistry and Catalysis
Debye Institute for Nanomaterials Science, Utrecht University
3854 CG, Utrecht (The Netherlands)
E-mail: p.e.dejongh@uu.nl

 Supporting information for this article is available on the WWW under <https://doi.org/10.1002/cctc.202001710>

 © 2021 The Authors. ChemCatChem published by Wiley-VCH GmbH. This is an open access article under the terms of the Creative Commons Attribution Non-Commercial NoDerivs License, which permits use and distribution in any medium, provided the original work is properly cited, the use is non-commercial and no modifications or adaptations are made.

Results and Discussion

Morphology of the ZnO catalysts

ZnO nanorods were grown on carbon paper via a low-temperature hydrothermal method^[28] (see experimental section for

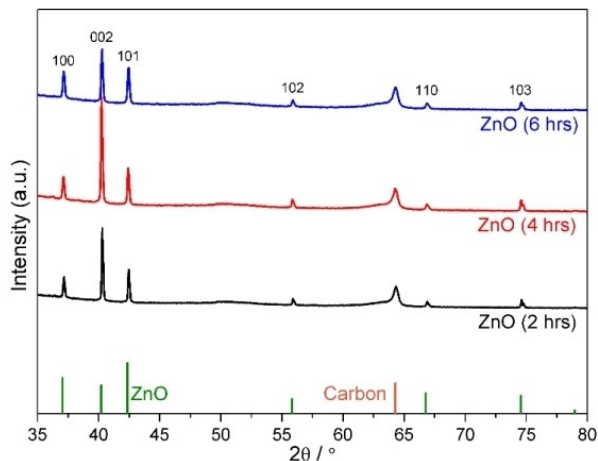


Figure 1. XRD patterns of the freshly prepared ZnO catalysts on carbon fiber paper.

details). To control the aspect ratios of the ZnO, the synthesis time was varied from 2 hrs, 4 hrs or 6 hrs, and the obtained ZnO catalysts were named ZnO (2 hrs), ZnO (4 hrs) and ZnO (6 hrs), respectively. Figure 1 shows the XRD patterns of ZnO (2 hrs), ZnO (4 hrs) and ZnO (6 hrs) catalysts on carbon fiber paper. All diffraction peaks match either those of carbon, or those of the wurzite ZnO structure (PDF card 00-036-1451).^[28] This shows that the synthesis method was successful in preparing crystalline ZnO. To further investigate the structure of the catalysts, scanning electron microscopy (SEM) images were acquired. As can be seen in Figure 2, all three catalysts; ZnO (2 hrs), ZnO (4 hrs) and ZnO (6 hrs), show a structure consisting of nanorods with a hexagonal shape and uniform size, which are well-distributed over the carbon paper. SEM images show that the length of the nanorods increased from about $5 \mu\text{m}$ to about $8 \mu\text{m}$ as the synthesis time was increased from 2 hrs to 4 hrs, but a further increase of the synthesis time to 6 hrs did not lead to further increase in size (Figure S2). However, a careful inspection revealed that the aspect ratio (ratio between the length and the width) for the nanorods increased with increasing synthesis time (Table S1).

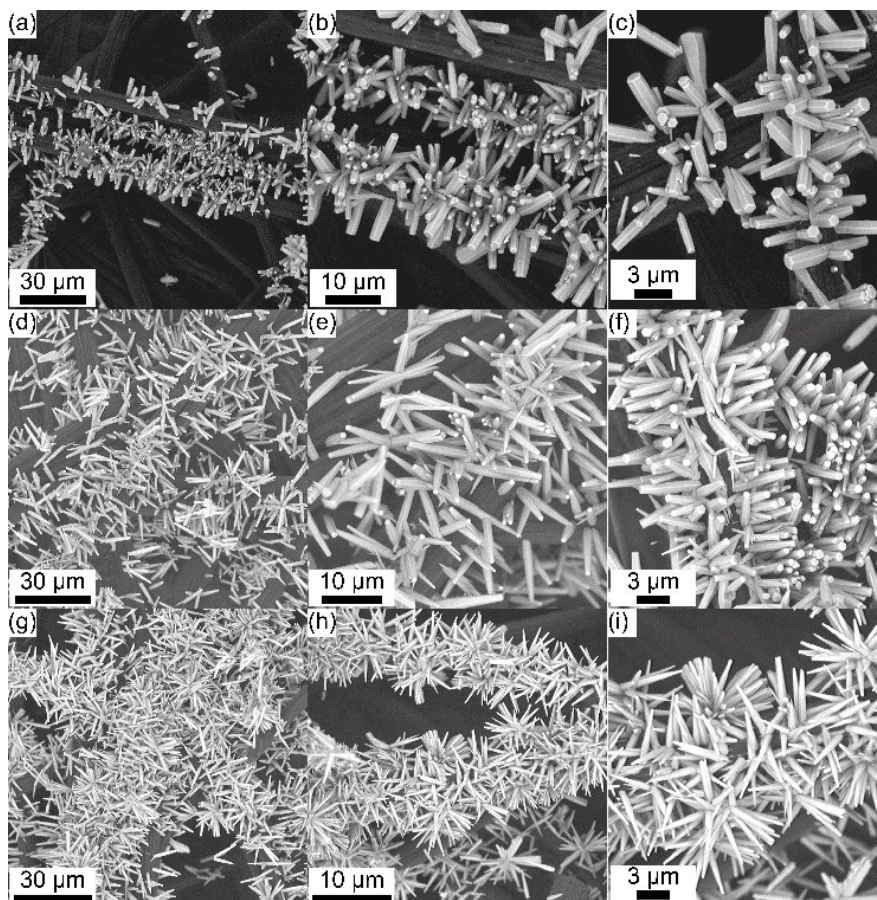


Figure 2. SEM images of freshly prepared ZnO catalysts: a, b, c) ZnO (2 hrs); d, e, f) ZnO (4 hrs); g, h, i) ZnO (6 hrs).

Reduction of ZnO to Zn

Zn catalysts were prepared by reducing the above ZnO nanorods at -1.0 V vs RHE for 10 mins in CO_2 saturated electrolytes (Table 1). Afterwards, the morphology and crystallinity of the reduced catalysts were analyzed using SEM and XRD, respectively. As shown in Figure 3, the initial ZnO nanorod morphologies were drastically changed after reduction. Specifically, the ZnO (2 hrs) became sponge-like (Figure 3a) after reduction in CO_2 saturated 0.5 M KHCO_3 . However, both ZnO (4 hrs) and ZnO (6 hrs) catalysts maintained their nanorod structure (Figure 3b) after the reduction treatment in CO_2 saturated 0.5 M KHCO_3 , except that the length was shortened from 8 μm to 5 μm (see Figure S3). Interestingly, when the ZnO nanorods (4 hrs and 6 hrs) were reduced in CO_2 saturated 0.1 M KClO_4 solution, they were transformed into metallic Zn nanoplates (Figure 3c).

In addition to the variation in the morphology, XRD showed pronounced differences in crystallinity after reduction of ZnO. For ZnO (2 hrs), apart from the carbon diffraction, no other diffraction peaks were observed after reduction (Figure 3d), confirming the amorphous nature of this reduced phase. XRD (Figure 3d) of the ZnO (4 hrs and 6 hrs) nanorods shows reduction to metallic Zn with a crystallite size of 46.5 ± 2 nm.^[29] Furthermore, when the ZnO nanorod (4 hrs and 6 hrs) were reduced in CO_2 saturated 0.1 M KClO_4 solution, they were also transformed into metallic Zn. For the nanoplates in particular, the Zn (101) reflection was more intense than both the Zn (002) and Zn (100) reflections, suggesting a preferential oriented Zn (101) facet. The Zn nanorods also show a slightly preferred Zn (101) orientation, but slightly less pronounced than for nanoplates (the ratio of (101)/(002) is 1.3 for the nanoplates, and 1.1 for the nanorods).

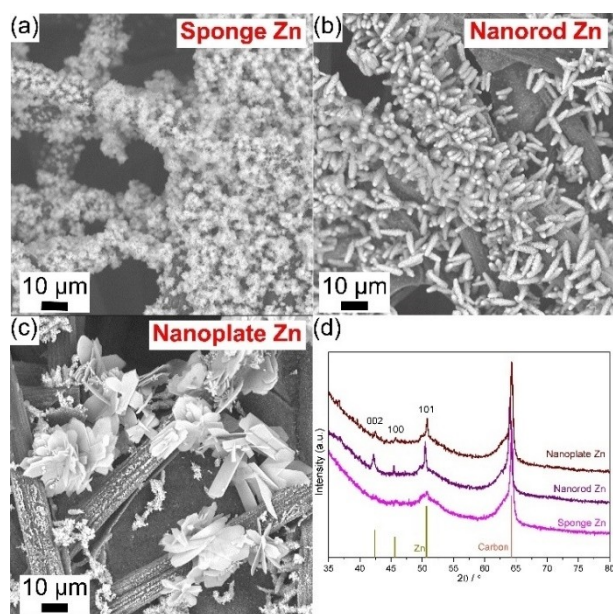


Figure 3. SEM images of the obtained a) sponge Zn, (b) nanorod Zn, (c) nanoplate Zn catalysts and the corresponding XRD patterns (d).

Furthermore, high resolution transmission electron microscopy (HRTEM) and the corresponding energy-dispersive X-ray spectroscopy (EDX) were performed to better understand the structure of the catalysts (Figure S4–7). As clear from the TEM-EDX results, the morphology of the as-prepared ZnO and reduced Zn catalysts are similar to the morphology observed by SEM. Specifically, ZnO catalyst shows homogeneously distributed Zn and O (Figure S4c and 4d). Regarding the reduced catalysts (Zn), the TEM/EDX shows that Zn is well-distributed over the carbon paper, but we still observed O in the Zn catalysts. This is expected as the Zn will be partially oxidized after the electrocatalytic reaction and during transfer to the TEM.

The difference in the structure of the catalysts reduced in the different electrolytes is intriguing. A first factor that plays a role is the pH of the solution, which influences the solubility and stability of the different phases. However, the pH of the bulk solution (0.5 M KHCO_3 , $\text{pH}=7.2$) was the same when obtaining either the sponge Zn or the nanorod Zn, suggesting that the pH effect is not the determining factor for the difference in structure. For the nanoplate Zn formed in 0.1 M KClO_4 , the bulk pH was more acidic ($\text{pH}=4.3$) than 0.1 M KHCO_3 ($\text{pH}=6.8$), therefore in this case differences in pH might have contributed to the different structure of the resulting Zn phase.

Another possible factor to explain the difference in structure (e.g. nanorod versus amorphous sponge Zn) of the Zn obtained by reduction in KHCO_3 is the difference in the initial size of the nanorods. It seems that the larger thickness of the ZnO (4 hr) and ZnO (6 hr) compared to the ZnO (2 hr) led to the preservation of the original rod-like structure. Perhaps, there is a certain thickness size below which crystalline Zn or the nanorod structure cannot be maintained during reduction. In fact, it is even surprising that the nanorod structure is maintained after electroreduction because ZnO and Zn have different crystalline structures.

A last factor that could be important is that the structural transformation during the reduction to the metal phase is the interaction between ZnO and specific anions. For instance, it has been reported that ClO_4^- ions can be adsorbed on the surface of ZnO, and one Cl would substitute an oxygen atom during the in situ electroreduction of the ZnO.^[30] This might explain why this anion substitution effect has not been observed for KHCO_3 as a strong interaction between ZnO and the HCO_3^- is not envisaged.^[31]

Electrochemical syngas and CO production

The oxide-derived Zn catalysts were tested for the CO_2 reduction in 0.5 M KHCO_3 electrolyte. The performance was first evaluated by linear sweep voltammetry (Figure 4 and S8). The bare glassy carbon electrode with and without carbon fiber paper was tested as a reference. If Zn was present, the current density was always higher than for the bare glassy carbon electrodes with or without carbon paper, and onset potentials for the H_2 evolution and CO_2 reduction were lower (Figure S8). Furthermore, the electrodes showed a higher current density in

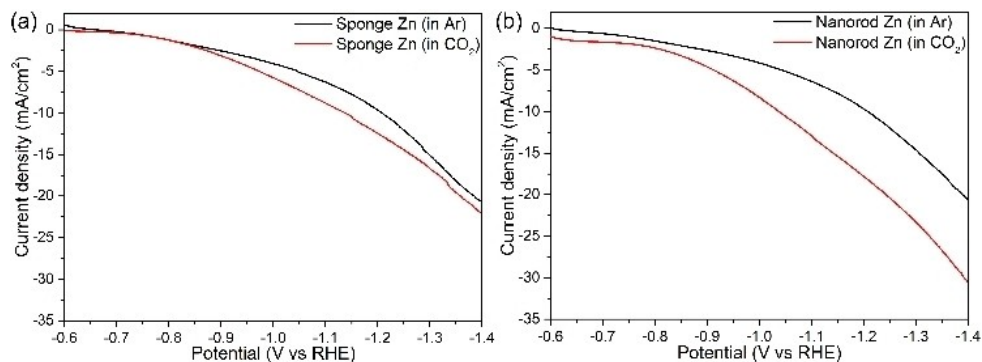


Figure 4. Linear sweep voltammetry of sponge-like Zn (a) and Zn nanorods (b) in both Ar and CO₂ atmosphere. Conditions: 0.5 M KHCO₃, 50 mV/s scan rate. The current density was normalized to the geometric area of 3.2 cm².

CO₂ than in Ar. We can hence conclude that these catalysts are active for electrochemical reduction of CO₂.

The selectivity was evaluated chronoamperometrically Zn in 0.5 M KHCO₃ at potentials between -0.7 V and -1.1 V vs RHE. The total experimental Faradaic efficiency (FE) as determined from the detected products was between 90% and 100%. In fact, the only at the start of the experiment some electrons were not used to create liquid or gaseous products, as they were used for the electroreduction of the remaining oxide species in the catalyst. The sponge-like Zn and nanorod showed syngas (a combination of H₂ and CO) as the main gas product, but with different H₂:CO ratios under the same experimental conditions (Figure 5a and 5b). Specifically, the sponge-like Zn showed a constant H₂:CO ratio of 2. Also, formate was

produced at all potentials between -0.8 V and -1.1 V (Figure 5a). The highest syngas Faradaic efficiency (FE_{syngas}) was 77% (50% H₂ and 27% CO) obtained at -0.8 V vs RHE, together with 8% formate production at a current density of 2.8 mA/cm². Applying the potential from -0.7 V to -1.1 V led to slightly higher formate selectivity (18% at -1.0 V vs RHE).

In contrast, the nanorod Zn catalyst produced only syngas; no formate was detected. As shown in Figure 5b, varying the potential from -0.7 V to -1.1 V (vs RHE), the FE of H₂ production decreased from 60% to 45%, while the FE of CO production increased from 30 to 45%. Surprisingly, the ratio between H₂ and CO remained 1 from -0.8 V to -1.0 V, and then decreased a bit at a higher overpotential. The actual syngas production rates were also calculated (Figure S10), and a

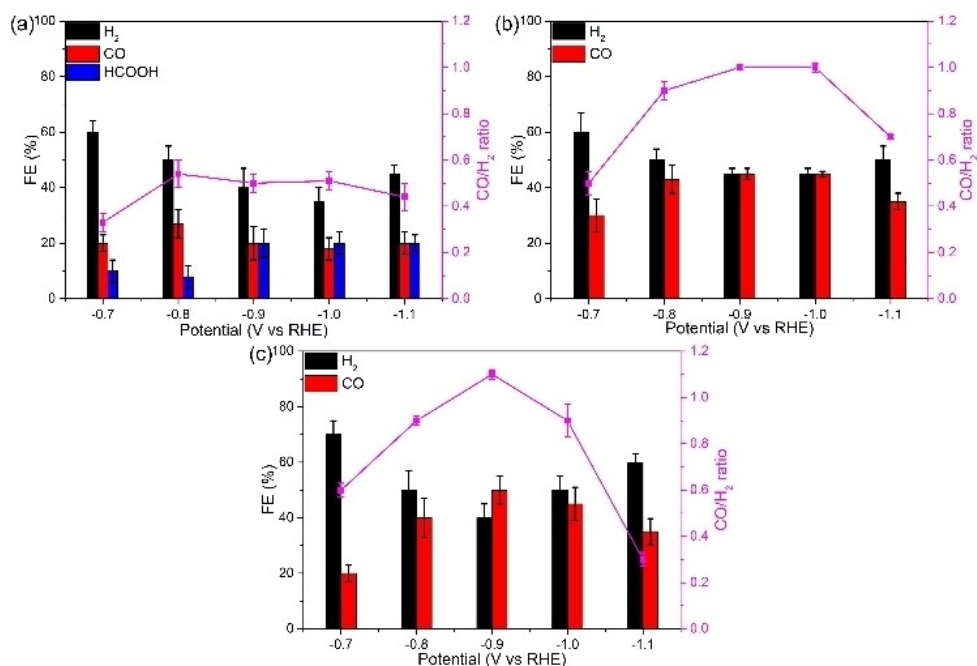


Figure 5. Faradaic efficiency of CO, H₂ and H₂:CO ratios for sponge Zn (a), nanorod Zn (b) and nanoplate Zn (c) in 0.5 M KHCO₃ at different potentials. (The error bar was obtained by repeating the experiments for at least three times).

rate of 0.48 mol/h/g was achieved at -1.1 V for the nanorod Zn catalyst. A longer test was conducted on the nanorod Zn catalyst (Figure S12), and the results reveal a slightly increased current density from 13 mA/cm² to 18 mA/cm² over 7 hours (the H₂:CO ratio remained at 1 ± 0.2), hence a reasonable stability of the catalyst. The ZnO (6 hrs) catalysts also produced syngas with a H₂:CO ratio around 1 (Figure S9), as it has a similar morphology,

Furthermore, we discuss the performance of the nanoplate Zn catalysts. Although they were formed in an KClO₄ electrolyte, for fair comparison they were thoroughly rinsed and their CO₂RR selectivity was measured in 0.5 M KHCO₃ as was done for the nanorods and sponge Zn catalysts (Figure 5c). Similar to the performance of nanorod Zn, the nanoplate Zn leads to syngas production, but with a CO:H₂ ratio ranging from 0.5 to 1.1 by changing the potential. Interestingly, the nanoplate Zn produces more CO (FE = 55%) than H₂ (FE = 40%) at -0.9 V, which can be attributed to the preferred Zn (101) orientation of the nanoplate structure.

These results show that the structural properties are a key factor for the performance of these Zn-based catalysts for electroreduction of CO₂ in water. In literature, it has been reported earlier that Zn catalysts consisting of small nanoparticles or amorphous Zn are more likely to produce formate.^[22,32] Thus, the production of formate and syngas from our sponge-like Zn can be explained by its amorphous nature, while our Zn nanorods with a higher crystallinity generate CO and H₂.

The effects of the electrolyte concentration on the performance of the catalysts was also investigated by using 0.1 M KHCO₃ instead of 0.5 M. Figure 6 gives an overview of the FE of the different catalysts using a 0.1 M KHCO₃ electrolyte at -1.0 V vs RHE with similar current density of 5.3 mA/cm². The results clearly demonstrate that the nanoplate Zn which exhibits dominant (101) facets, produces mostly CO (FE = 85%) at -1.0 V vs RHE with a current density of 5.3 mA/cm², corresponding to 0.20 mol/h/g CO production. On the other hand, the nanorod Zn with mixed facets and the amorphous Zn

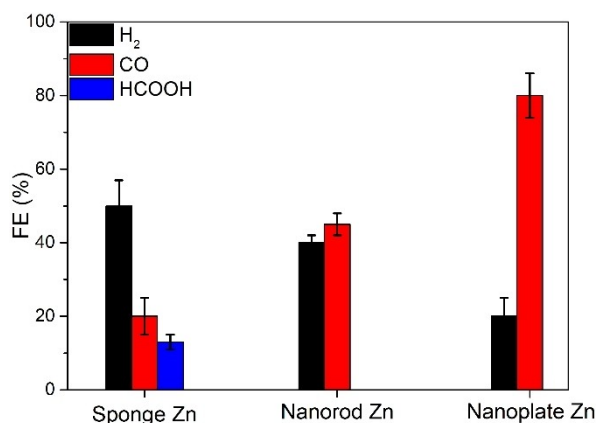


Figure 6. Faradaic efficiency for CO and H₂ obtained at -1.0 V obtaining 5.3 ± 0.3 mA/cm² in CO₂ saturated 0.1 M KHCO₃ for different types of Zn catalysts.

produce syngas (a mixture of H₂ and CO) under the same conditions. Furthermore, the lower HCO₃⁻ concentration apparently benefits the CO production for both nanorod Zn and nanoplate Zn. By comparing the three catalysts, the high CO production of the nanoplate Zn can be attributed to abundance of Zn (101) facets and higher crystallinity of this catalyst compared to the Zn nanorods and the Zn sponge. Differences in the local pH are not expected to significantly contribute to the difference in the catalysts' performance; as the currents drawn are small, for all catalysts we do not expect a significant difference between the local pH and the bulk pH during the reaction.^[33]

What determines the performance?

It is clear from the CO₂ reduction results presented above that the three different structures of the Zn catalysts exhibit different selectivities in CO₂ reduction. It is generally known that current densities, and hence active site densities, can influence selectivity e.g. via local pH variations or concentration gradients. In order to verify whether the observation is related to local current densities, the electrochemically active surface areas of the catalysts were determined, based on the double-layer capacitance (C_{dl}).^[34,35]

Figure 7 shows the charging current densities at different scanning rates for the three different catalysts in 0.1 M KHCO₃, since we normalized and compared the three catalysts at this condition. Firstly, it is observed that the nanorod Zn has a C_{dl} about two times higher than the Zn sponge. The C_{dl} derived from the data shown in Figure 7a is larger for the Zn nanorod catalyst than for the sponge Zn catalyst, indicative of a higher electrochemical surface area for the nanorods. One would expect a higher bulk surface area for sponge Zn (Figure 3), but this is not the case. The ECSA-normalized CO partial current density versus the applied potentials (j_{CO}) (Figure 7b) gives a similar j_{CO-ECSA} for the two catalysts at low overpotentials. This suggests that they have similar intrinsic activity, but the different selectivity is probably due to differences in the densities of the active sites in the Zn catalysts.

Secondly, Figure 7a shows that the obtained C_{dl} for Zn nanoplates is higher than sponge Zn, but lower than nanorod Zn. The ECSA-normalized CO partial current density shows that the nanoplate Zn exhibits the highest CO partial current density (Figure 7b), suggesting that the improved CO production by the nanoplate Zn is essentially due to higher intrinsic activity of nanoplate Zn. Besides, the SEM and XRD results indicate that the Zn nanoplates have more exposed (101) facets than the Zn nanorods (the intensity ratio of (101)/(002) is 1.3 for nanoplates, and 1.1 for nanorods), and it is reported that the Zn (101) facet is beneficial for CO₂ activation due to a lower energy barrier.^[19] Therefore, we attribute the difference in selectivity for Zn nanoplate to the difference in the exposed facets (leading to different intrinsic activity), rather than a different densities of active sites.

Additional information about the mechanism can be obtained from the Tafel plot. A Tafel slope of 118 mV/dec

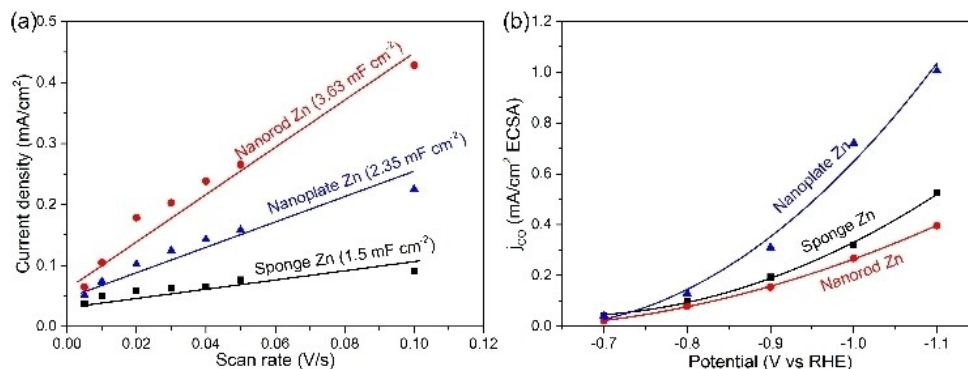


Figure 7. Charging current densities against scan rates (a) and electrochemical surface area normalized CO partial current density (b) for sponge Zn, nanorod Zn and nanoplate Zn catalysts in 0.1 M KHCO_3 . (The cyclic voltammetry measurements at different scan rates for different catalysts are shown in Figure S13 and S14).

supports the formation of CO_2^{*-} intermediate, showing that the initial electron transfer is the rate-determining step, while a slope of 59 mV/dec means that protonation of CO_2^{*-} is the rate-determining step.^[36] As shown in Figure S16, the Zn sponges and Zn nanorod catalysts show a Tafel slope close to 118 mV/dec, implying that initial electron transfer is the rate-determining step for both catalysts, but the Zn sponge has a slightly lower slope (110 mV/dec) than the nanorods (129 mV/dec). Interestingly, a similar comparison between the nanorods and nanoplates in 0.1 M KHCO_3 (Figure S16b) shows a lower slope for the Zn nanoplates than for the nanorods and sponge Zn (128 mV/dec versus 159 mV/dec). These results are indicative of slightly faster kinetics for CO_2 interaction with Zn nanoplates than with the nanorods. Thus, the results of the Tafel plots support our interpretation of the observed differences in selectivity of these catalysts.

Conclusion

In summary, ZnO nanorod electrocatalysts with different aspect ratios were synthesized by hydrothermal techniques. We showed that the initial morphology of the ZnO nanorod and the type of electrolyte medium had a huge impact on the final structure of the active Zn catalysts and determined the activity and product selectivity during electrochemical CO_2 reduction. Zn nanoplates achieved the highest CO selectivity; up to 85% at -1.0 V. This study demonstrates how the initial morphology of metal oxide catalysts changes during the CO_2 RR, and how the resulting structure determines the active phases and the performance of the catalysts.

Experimental Section

ZnO nanorod preparation. ZnO was grown on carbon paper (TGP-H-060) using a low-temperature hydrothermal method.^[28] Typically, a piece of carbon paper disc ($r = 1$ cm) was immersed into an aqueous solution containing 0.05 M $\text{Zn}(\text{NO}_3)_2$ and 0.05 M hexamethylenetetramine, then the solution was kept at 85°C for

2 hrs, 4 hrs or 6 hrs. Subsequently, the carbon paper was washed with water and dried at room temperature. The obtained ZnO catalysts were named ZnO (2 hrs), ZnO (4 hrs) and ZnO (6 hrs), respectively. The final loading of the catalysts was verified by ICP measurements, and the loadings were 0.18 mg/cm^2 , 0.36 mg/cm^2 , 0.42 mg/cm^2 for ZnO (2 hrs), ZnO (4 hrs) and ZnO (6 hrs), respectively.

Zn preparation. Zn catalysts were prepared by reducing the above ZnO at -1.0 V vs RHE for 10 mins in different CO_2 saturated electrolytes, and the specific conditions are in the below Table 1.

Structural characterization. XRD measurements were performed with a Bruker D2 Phaser, with a $\text{Co K}\alpha$ X-ray source ($\lambda = 1.79026\text{ \AA}$). The XRD measurements were conducted at a 2θ range from 35° to 80° , using 1 s as the integration time. Scanning electron microscopy analysis was performed on a Phenom ProX scanning electron microscope (operating at 10 keV). Bright field transmission electron microscopy (TEM) and dark field scanning transmission electron microscopy (STEMEDX) images were acquired at a FEI Talos F200X microscope operated at 200 kV equipped with 4 energy dispersive X-ray (EDX) detectors, a high-angle annular dark-field (HAADF) and a bright field detector. The ICP analysis was carried out using a Perkin-Elmer AAS Model Analyst 200, and the measurement was conducted at MIKROLAB (Mikroanalytisches Labor Kolbe, c/o Fraunhofer Institut UMSICHT, Germany).

Electrochemical measurements. The electrochemical experiments were performed in an H-type cell (Figure S1) with an Autolab potentiostat (PGSTAT AT204). In the cell, the cathode part and anode part were separated by a Nafion membrane (Nafion™ Membrane XL, Ion Power, GmbH), and both were filled with an aqueous 11 mL KHCO_3 solution as the electrolyte. In the cell configuration, the carbon paper supported ZnO catalyst was attached onto a piece of glassy carbon electrode, because of the fragility of the carbon fiber paper. Ag/AgCl (3 M KCl) was used as a reference electrode, and a Pt disk was used as the counter electrode. The exposed geometric area of both working electrode and Pt counter electrode is 3.2 cm^2 .

Table 1. The specific experimental conditions for different Zn catalysts.			
Zn structure	ZnO precursor	Electrolyte (CO_2 saturated)	Current density
Sponge Zn	ZnO (2 h)	0.5 M KHCO_3	11.5 mA/cm^2
Nanorod Zn	ZnO (4 h/6 h)	0.5 M KHCO_3	13.3 mA/cm^2
Nanoplate Zn	ZnO (4 h)	0.1 M KClO_4	5.3 mA/cm^2

Before testing, the cathodic and anodic parts were flushed with CO₂ and Ar respectively (both 10 mL/min) for 30 mins, and both gas flow were maintained during the CO₂ electroreduction measurements. All the potential values with respect to Ag/AgCl were converted to potentials with respect to the reversible hydrogen electrode potential. IR corrections were applied, based on the measured impedance of both 0.5 M KHCO₃ and 0.1 M KHCO₃ solutions. Impedance measurements were performed using a Princeton Applied Research Parstat 2273, a 20 mV rms modulated AC potential with frequencies from 1 MHz to 1 Hz was used. The uncompensated resistances were 5 Ω/cm for 0.5 M KHCO₃ and 26 Ω/cm for 0.1 M KHCO₃.

Gaseous products were analyzed by connecting the outlet of the cathode compartment to a Global Analysis Solutions Microcompact GC 4.0. The GC system was equipped with 3 detector channels (2 FID and 1 TCD): The first channel has a Rt-Q Bond (10 m*0.32 mm, Agilent) packed column and a FID detector for the detection of CH₄, C₂H₄ and C₂H₆, the second channel has Molecular Sieve 5 A (10 m* 0.53 mm, Restek) packed column that separates small gaseous molecules such as CO, and CH₄. This channel has a FID detector with a methanizer to increase the detection sensitivity of CO. The third channel has a Carboxen 1010 (8 m*0.32 mm, Agilent) packed column which separates H₂ and CO₂ with a TCD. High purity nitrogen (N₂, 99.999%) was used as a carrier gas.

Liquid phase products in the catholyte were verified using a Varian HPLC equipped with a refractive index detector and a Bio-Rad Aminex HPX-87H column at 65 °C. 1 mM H₂SO₄ was used as the eluent with a flow rate of 0.55 mL/min. The retention time of formic acid was 15 min and the total analysis time was 20 minutes.

Acknowledgements

This work was supported by the European Research Council; project number ERC-2014-CoG 648991. The Solar-to-Products program funded by the Dutch Research Council (NWO) is acknowledged for funding. Marisol Tapia Rosales, Francesco Mattarozzi and Jan Willem de Rijk are acknowledged for useful discussions on the electrochemical set-up and measurements. Min Tang is acknowledged for performing the TEM/EDX measurements.

Conflict of Interest

The authors declare no conflict of interest.

Keywords: CO₂ electroreduction · ZnO nanorods · Reduced Zn phase · Structure depended selectivity · Multiple products

- [5] Y. J. Zhang, V. Sethuraman, R. Michalsky, A. A. Peterson, *ACS Catal.* **2014**, *4*, 3742–3748.
- [6] K. P. Kuhl, T. Hatsukade, E. R. Cave, D. N. Abram, J. Kibsgaard, T. F. Jaramillo, *J. Am. Chem. Soc.* **2014**, *136*, 14107–14113.
- [7] R. Kortlever, J. Shen, K. J. P. Schouten, F. Calle-Vallejo, M. T. M. Koper, *J. Phys. Chem. Lett.* **2015**, *6*, 4073–4082.
- [8] Y. Hori, A. Murata, K. Kikuchi, S. Suzuki, *J. Chem. Soc. Chem. Commun.* **1987**, 728–729.
- [9] S. Ikeda, T. Takagi, K. Ito, *Bull. Chem. Soc. Jpn.* **1987**, *60*, 2517–2522.
- [10] N. Hoshi, M. Kato, Y. Hori, *J. Electroanal. Chem.* **1997**, *440*, 283–286.
- [11] C. E. Tornow, M. R. Thorson, S. Ma, A. A. Gewirth, P. J. A. Kenis, *J. Am. Chem. Soc.* **2012**, *134*, 19520–19523.
- [12] D. Gao, H. Zhou, J. Wang, S. Miao, F. Yang, G. Wang, J. Wang, X. Bao, *J. Am. Chem. Soc.* **2015**, *137*, 4288–4291.
- [13] Y. Hori, in *Mod. Asp. Electrochem.* (Eds.: C. G. Vayenas, R. E. White, M. E. Gamboa-Aldeco), Springer New York, New York, NY, **2008**, pp. 89–189.
- [14] R. Kas, K. K. Hummadi, R. Kortlever, P. De Wit, A. Milbrat, M. W. J. Luiten-Olieman, N. E. Benes, M. T. M. Koper, G. Mul, *Nat. Commun.* **2016**, *7*, DOI 10.1038/ncomms10748.
- [15] H. S. Jeon, S. Kunze, F. Scholten, B. Roldan Cuenya, *ACS Catal.* **2018**, *8*, 531–535.
- [16] K. Liu, J. Wang, M. Shi, J. Yan, Q. Jiang, *Adv. Energy Mater.* **2019**, *9*, 1–6.
- [17] Y. Hori, K. Kikuchi, S. Suzuki, *Chem. Lett.* **1985**, *14*, 1695–1698.
- [18] S. Ikeda, A. Hattori, M. Maeda, K. Ito, H. Noda, *Electrochemistry* **2000**, *68*, 257–261.
- [19] D. H. Won, H. Shin, J. Koh, J. Chung, H. S. Lee, H. Kim, S. I. Woo, *Angew. Chem. Int. Ed.* **2016**, *55*, 9297–9300; *Angew. Chem.* **2016**, *128*, 9443–9446.
- [20] B. Qin, Y. Li, H. Fu, H. Wang, S. Chen, Z. Liu, F. Peng, *ACS Appl. Mater. Interfaces* **2018**, *10*, 20530–20539.
- [21] P. Moreno-García, N. Schlegel, A. Zanetti, A. Cedeno López, M. D. J. Gálvez-Vázquez, A. Dutta, M. Rahaman, P. Broekmann, *ACS Appl. Mater. Interfaces* **2018**, *10*, 31355–31365.
- [22] T. Zhang, X. Li, Y. Qiu, P. Su, W. Xu, H. Zhong, H. Zhang, *J. Catal.* **2018**, *357*, 154–162.
- [23] Y. Chen, C. W. Li, M. W. Kanan, *J. Am. Chem. Soc.* **2012**, *134*, 19969–19972.
- [24] A. Dutta, A. Kuzume, M. Rahaman, S. Vesztergom, P. Broekmann, *ACS Catal.* **2015**, *5*, 7498–7502.
- [25] S. Gao, Y. Lin, X. Jiao, Y. Sun, Q. Luo, W. Zhang, D. Li, J. Yang, Y. Xie, *Nature* **2016**, *529*, 68–71.
- [26] A. Verdager-Casadevall, C. W. Li, T. P. Johansson, S. B. Scott, J. T. McKeown, M. Kumar, I. E. L. Stephens, M. W. Kanan, I. Chorkendorff, *J. Am. Chem. Soc.* **2015**, *137*, 9808–9811.
- [27] O. Fruhwirth, J. Friedmann, G. W. Herzog, *Surf. Technol.* **1976**, *4*, 417–429.
- [28] M. Law, L. E. Greene, J. C. Johnson, R. Saykally, P. Yang, *Nat. Mater.* **2005**, *4*, 455–459.
- [29] K. Jiang, H. Wang, W.-B. Cai, H. Wang, *ACS Nano* **2017**, *11*, 6451–6458.
- [30] J. Rousset, F. Tsin, M. Guc, J. Vidal, A. Le Bris, A. Thomere, V. Izquierdo-Roca, D. Lincot, *J. Phys. Chem. C* **2016**, *120*, 18953–18962.
- [31] F. Quan, D. Zhong, H. Song, F. Jia, L. Zhang, *J. Mater. Chem. A* **2015**, *3*, 16409–16413.
- [32] T. Zhang, H. Zhong, Y. Qiu, X. Li, H. Zhang, *J. Mater. Chem. A* **2016**, *4*, 16670–16676.
- [33] K. Yang, R. Kas, W. A. Smith, *J. Am. Chem. Soc.* **2019**, *141*, DOI 10.1021/jacs.9b07000.
- [34] E. L. Clark, J. Resasco, A. Landers, J. Lin, L.-T. Chung, A. Walton, C. Hahn, T. F. Jaramillo, A. T. Bell, *ACS Catal.* **2018**, *8*, 6560–6570.
- [35] F. Song, X. Hu, *Nat. Commun.* **2014**, *5*, DOI 10.1038/ncomms5477.
- [36] M. Dunwell, W. Luc, Y. Yan, F. Jiao, B. Xu, *ACS Catal.* **2018**, *8*, 8121–8129.

[1] J. M. Spurgeon, B. Kumar, *Energy Environ. Sci.* **2018**, *11*, 1536–1551.

[2] B. M. Tackett, W. Sheng, J. G. Chen, *Joule* **2017**, *1*, 253–263.

[3] T. Zheng, K. Jiang, H. Wang, *Adv. Mater.* **2018**, *30*, 1–15.

[4] D. T. Whipple, P. J. A. Kenis, *J. Phys. Chem. Lett.* **2010**, *1*, 3451–3458.

Manuscript received: November 20, 2020

Revised manuscript received: January 20, 2021

Accepted manuscript online: January 22, 2021

Version of record online: February 24, 2021